Groundwater-induced flooding in macropore-dominated hydrological system in the context of climate changes

J.-L. Pinault, Nadia Amraoui, C. Golaz

Groundwater-induced flooding in macropore-dominated hydrological system in the context of climate changes

J.-L. Pinault, N. Amraoui, and C. Golaz

Water Research Division, Bureau de Recherches Géologiques et Minières, Orléans, France

Received 9 April 2004; revised 11 January 2005; accepted 28 January 2005; published 3 May 2005.

[1] The groundwater-induced flooding that occurred in the Somme Basin during April 2001 damaged numerous dwellings and communication routes, and economic activity of the region was flood-bound for more than 2 months. It was the first time that such a sudden event was recognized as resulting from groundwater discharge, despite the Somme valley not being prone to flooding. Because of a dual porosity of the chalk in the basin, nonlinear processes, involving a hydraulic continuity between the macropores of the unsaturated zone and the chalk groundwater, govern water migration through the unsaturated zone. Such a process is the result of switching behavior of groundwater recharge from matrix flow to macropore flow due to accumulated wetness over several years. There is much evidence to support that the flood probability model is climate-dependent for the studied region because nonlinear processes amplify the effects of nonstationarities of climatic inputs. An estimation of the return period of catastrophic flooding depends on the long-term precipitation fluctuations. This has implications for flood risk assessment requiring the need to distinguish between short- and long-term flooding risks. Other basins that may not appear particularly prone to flooding could also be subjected to similar groundwater-induced flooding should the long-term precipitation fluctuations observed in the north of France since the beginning of the 1980s persist. Similar extraordinary situations can occur in Belgium and England, whereby significant flooding results in substantial contribution of groundwater flows.

Citation: Pinault, J.-L., N. Amraoui, and C. Golaz (2005), Groundwater-induced flooding in macropore-dominated hydrological system in the context of climate changes, *Water Resour. Res.*, *41*, W05001, doi:10.1029/2004WR003169.

1. Introduction

[2] The analysis of flood frequency has developed considerably over the past few years, including the link between flooding and climate changes [*Georgakakos et al.*, 1998; *Boyle et al.*, 2001; *Blazkova and Beven*, 2002; *Chandler and Wheater*, 2002; *Goel et al.*, 2000; *Jain and Lall*, 2001; *Franks and Kuczera*, 2002; *Latraverse et al.*, 2002; *Morrison and Smith*, 2002] and analysis and simulation of precipitation [*Buishand and Brandsma*, 2001; *Cowpertwait et al.*, 2002; *Veneziano and Iacobellis*, 2002]. Most of the studies are devoted to the analysis of floods due to runoff that is induced by exceptional rainfalls. The groundwater-induced flooding process that is presented here is the result of switching behavior of groundwater recharge from matrix flow to macropore flow in a chalk aquifer due to accumulated wetness over several years.

[3] Flood generation mechanisms are studied to forecast the Somme catchment response in the context of climate changes. In addition to the precipitation fluctuations at different timescales, the role of the unsaturated zone where nonlinear processes occur is considered. Because of the chalk aquifer having a dual porosity, groundwater head can increase drastically in some parts of the catchment when, the matrix being close to saturation, hydraulic continuity is established between the micropores and the macropores. Discharge is extremely rapid where both hydraulic gradients are steep and permeability values increase toward the valley. Thus nonlinear processes amplify the effects of nonstationarities of climatic inputs. Moreover, flood prediction in nonlinear hydrosystems considerably increases uncertainty and the reliability of forecasting.

[4] Using inverse transfer models interfaced with rainfall and potential evapotranspiration generators, we are able to quantify the incidence of the increase in long-term precipitation fluctuations observed since the 1980s upon the return interval of the groundwater-induced flooding that occurred in the Somme valley in France during the spring of 2001. We find that mechanisms of rainwater transfer to the Somme River makes the Somme basin particularly sensitive to multiyear rainfall fluctuations. As such, this basin can be considered as an indicator of climate changes, owing to the extreme rarity of groundwater-induced flooding in the Somme valley.

[5] Indeed, in his exhaustive compilation, *Champion* [2001] relates that before the 17th century, no document mentions extraordinary floods in the Somme valley. Some floods have occurred ever since. Although some of them were severe, they were all characterized by their briefness, with most occurring in winter related to the breakup of ice in rivers [*Deneux and Martin*, 2001; *Hubert*, 2001; *Lefrou*, 2001]. Anthropic modifications in the catchment seem not be able to have contributed significantly to the 2001 flood,

0043-1397/05/2004WR003169

including transfers between the Seine and the Somme basins via the ''Canal du Nord'' and the ''Canal de St Quentin''.

[6] To analyze the response of the Somme flow to nonstationarities of climatic inputs, a stochastic process is developed using a rainfall generator such that precipitation fluctuations are controlled at different timescales as well as a potential evapotranspiration generator. For every simulated rainfall and evapotranspiration series, a nonlinear transfer model produces piezometric level and streamflow series. The statistic analysis of simulated streamflow series allows specifying the relation of causality between precipitation fluctuations at different timescales and groundwater-induced flooding. A sensitivity analysis of the basin is carried out according to different hypotheses on climate evolution.

2. Field Description

[7] The Somme Basin, which belongs to the northern aureole of the Paris Basin [*Amraoui et al.*, 2002], shows certain similarities to other basins of northern Europe [*Wellings*, 1984; *Gardner et al.*, 1990; *Crampon et al.*, 1993; *Price et al.*, 1993]. From base to top the stratigraphic succession comprises (1) Early and Middle Turonian marl, (2) Late Turonian and Senonian chalk, (3) Tertiary sands and clays, and (4) Quaternary alluvium in the valleys and silt on the plateaus. The catchment of the Somme River, extending over 5560 km^2, is composed of complex hydrosystems, including ponds and marshes that have undergone major transformation over previous centuries. Groundwater is discharged toward the main valleys and the tributaries are permanently fed; a strong correlation exists between the pressure head of the chalk groundwater and surface water flow. The rainfall in winter determines groundwater recharge. The main aquifer is composed of Late Turonian and Senanian chalk and, more locally in the wet valleys, riverbank sediments comprising sand, gravel and ancient alluvium. Middle and Early Turonian marl forms the lower confining bed. Aquifer thickness varies between 20 and 200 m. Effective porosity is about 5–8%, including fissures (1%) responsible for macropermeability. The fissures are the result of solution opening, open joints, fractures and faults. The distribution of fracture porosity is extremely heterogeneous, varying from very low beneath the plateaus, to more developed in the dry valleys, and commonly very high in the wet valleys where it can reach 30%. Fracture porosity decreases gradually as depth increases and finally disappears totally. The compact and impermeable chalk forms the lower confining bed of the fissured chalk. Transmissivity varies from 1.5×10^{-4} to 1.1×10^{-3} m^2/s under the plateaus, 6.8×10^{-3} to 2.7×10^{-2} m^2/s under the dry valleys, and 2.7×10^{-2} to 2.1×10^{-1} m^2/s under the wet valleys. The thickness of the unsaturated zone varies considerably from 1 m in the wet valleys where the groundwater head is constrained by the surface water network, to between 5 and 25 m under the dry valleys, and between 30 and 60 m under the plateaus. The unsaturated zone is relatively thin under the Santerre plateau (about 20 m) but can reach 80 m in some places of the Somme Basin. Altitude of the water table varies from 5 m in the low valleys of the Somme to 210 m [*Roux*, 1978] (Figure 1).

[8] Study of the piezometric level shows that (1) the chalk water table mimics the morphology of the topography, thus damping any irregularities, (2) the chalk groundwater seeps toward the main valleys, which behave as the base level, and permanently feeds the tributaries, (3) the riverbank sediments and the chalk aquifer are continuous in the wide Somme valley, and (4) the structure of the lower confining bed influences the piezometric pattern, meaning that the water table is very flat under the Santerre plateau whereas anticlines of the marl induce piezometric ridges. The hydraulic gradient varies considerably throughout the basin, strongly influenced by both aquifer permeability and topography (Figure 1).

3. Analysis of Rainfall Events at Different Timescales

[9] Figure 2 represents the aggregated rainfall height at different timescales. Short-term exceptional events occurred after the flooding, but their consequence was limited because of their sporadic nature. The depth of precipitation reached 95.2 mm from 6 to 7 July 2001 and 120.2 mm from 1 to 10 of November 2002, whereas no rainfall episode had been recorded at 95 mm using a 10-day sampling rate over the entire 20th century (Figure 2a). With a 2-month step, the mean value from 1900 to 2002 is 109 mm. Rainfall height reached 246 mm (March–April 2001), 250 mm after flooding (November–December 2002). Upper values were reached in 1930s without inducing catastrophic flooding (Figure 2b). With a 1-year step, rainfall height reached 922 mm (July 2000 to June 2001), whereas mean rainfall from 1900 to 2002 is only 648 mm. This 274 mm excess had nonetheless been previously reached (1930–1931, 1936–1937, 1923–1924), even exceeded, but had not been accompanied by catastrophic flooding. The Somme flow, which slightly exceeded 80 m^3/s in March 1931, reached 104 m^3/s in 2001 whereas the average flow at Abbeville varies between 20 and 60 m^3/s. The exceptional rainfall conditions become more obvious when data are plotted over two consecutive years rather than one (Figure 2d). The cumulated rainfall height reached 1646 mm in 1999–2000, then 1746 mm in 2001–2002, whereas the expected value is 1285 mm for the period extending from 1900 to 2002. Both consecutive values are records; the years 1965–1966 were very wet (cumulated rainfall reached 1597 mm), but this followed two years slightly in deficit. Consequently, it is not the cumulated rainfall over 2000 or 2001 that is exceptional, but the accumulated wetness over two years. Thus the catastrophic flooding of 2001 seems to be explained by the long-term rainfall behavior.

4. Role of the Unsaturated Zone in Groundwater-Induced Flooding

[10] Nevertheless, exceptional rainfall alone cannot explain the large volume of water that was discharged via the river in 2001. For the first semester of 2001, the mean Somme flow was therefore 84.0 m^3/s whereas only 72.7 m^3/s resulted from the precipitation that felt on the catchment, hence a 0.18 km^3 water excess, equivalent to 32 L/m^2 evenly distributed over the catchment. Such nonlinearities cannot be explained from runoff due to the very long regulation time of the process. So, nonlinear processes of water transfer in the unsaturated zone have to be integrated into the model. A dual porosity, interstitial porosity and fracture porosity characterizes the chalk. This behavior is

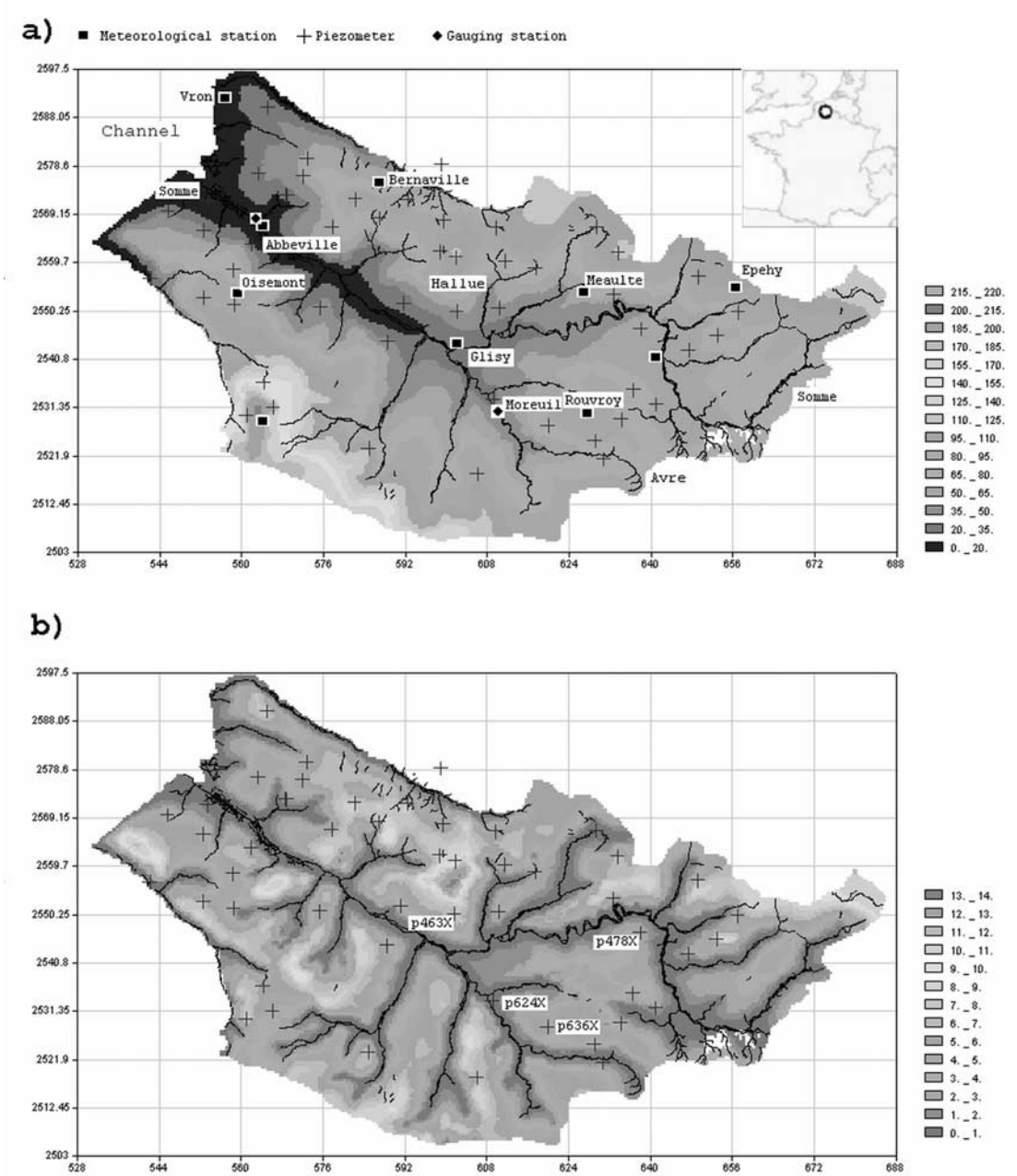

Figure 1. (a) Piezometric map and some equipment of the Somme Basin. Piezometric levels are calculated from 57 piezometers (hydrodynamic modeling with MARTHE software [*Amraoui et al.*, 2003; *Thiery et al.*, 2004]). Among the meteorological stations the Glisy station has produced data since 1900 with an interruption during the first World War. (b) Piezometric map and some equipment of the Somme Basin. Difference in piezometric levels between April 2001 (high storage) and December 2000 (low storage) is shown. The piezometers whose increase anticipated the flooding of April 2001 are located on the slopes of the wet valleys. See color version of this figure at back of this issue.

specific to the chalk, which shows both a very fine porosity network and a well-organized fracture network on a large scale. Water content in the interstitial porosity is always close to saturation due to both water migration downward to the water table and the capillary fringe. After abundant rainfall, an increase in capillary pressure leads to saturation of the conductive fractures, which occurs when the water content exceeds a certain threshold [*Wellings*, 1984; *Peters and Klavetter*, 1988; *Price et al.*, 2000; *Mahmood-ul-Hassan and Gregory*, 2002; *Haria et al.*, 2003]. Below this threshold, water is only slightly mobile because it is trapped in the fine pores of the chalk.

5. Mathematical Modeling and Numerical Analysis

[11] A stochastic process is developed from which statistic analysis of simulated streamflow allows the calculation

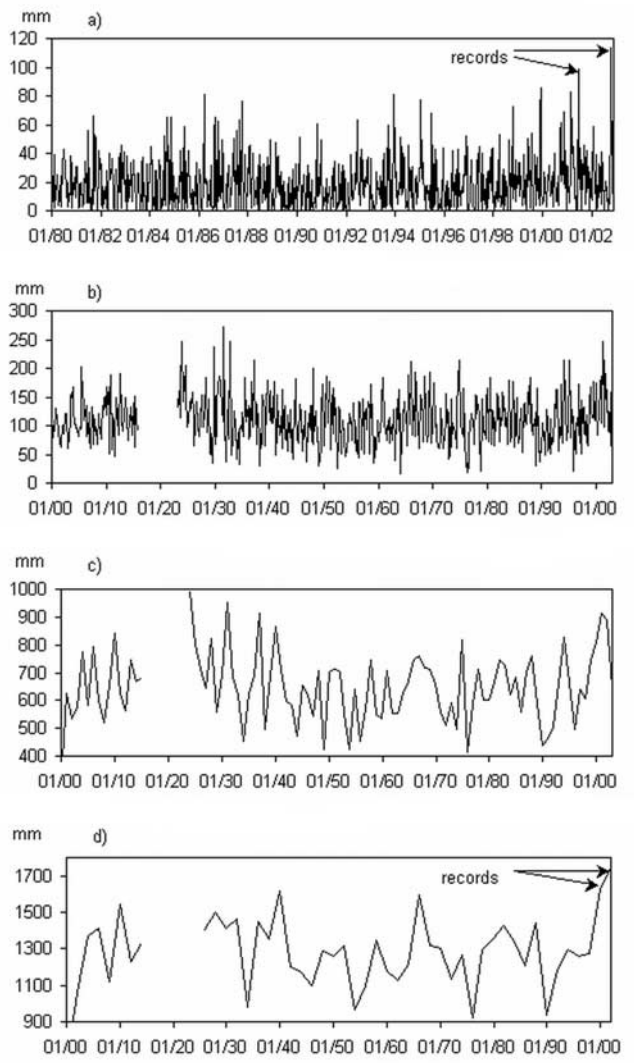

Figure 2. Representation of rainfall height aggregated over (a) 10 days, (b) 2 months, (c) 1 year, and (d) 2 years (Glisy station).

of the probability of occurrence of catastrophic flooding. As inputs of the process both rainfall and evapotranspiration series lead to streamflow series via a transfer model. The rainfall generator produces series of precipitation whose variability is controlled for different timescales. The evapotranspiration generator is coupled to the rainfall generator to simulate realistic climatic conditions. A transfer model whose architecture is shown in Figure 3 is composed of three elements in cascade. Two nonlinear transfer models aim to represent piezometric levels, the outputs of which are used as inputs for the third linear model that represents the Somme flow at Abbeville. This organization allows the quantification of processes, showing the contribution of (1) quick and delayed transfer modes through the unsaturated zone leading to groundwater recharge and (2) groundwater discharge and runoff.

[12] Data processing is done using the TEMPO code [*Pinault*, 2001]. Modeling is carried out with a 10-day sampling step, which minimizes discrepancies between the models and observations.

5.1. Taking into Account Groundwater Into the Somme Flow Transfer Model

[13] The inverse transfer model aims at estimating impulse responses of the Somme flow from pressure head measurements and effective rainfall obtained from different meteorological station data, the purpose being hydrograph separation, i.e., the decomposition of the Somme flow into components related to runoff and groundwater discharge. The contribution of groundwater to surface water flow can be calculated accurately provided that the piezometers are implemented so that they reflect the relations of groundwater-river water [*Pinault et al.*, 2001a, 2001b]. Piezometers are installed on the slopes and near the edge of the plateaus in order to characterize the drainage processes of groundwater to the surface water network (Figure 1b). The piezometric variations of p463X in the Hallue catchment (Figure 4a) reflect closely the Somme flow, which proves that the Somme is mainly fed by the fissured chalk aquifer. In particular, the pressure head variations that were observed for this piezometer anticipated the exceptional flooding of 2001. Other piezometers located at the top of the wet valley sides exhibited similar responses. A decrease in pressure head after flooding is more or less delayed depending on the degree of chalk weathering (Figure 4). Although the piezometric level of the groundwater in the Avre valley fed by the Santerre plateau increased as rapidly as in the fissured chalk aquifer during flooding, it decreased slower afterward, before increasing again for winter 2001/2002.

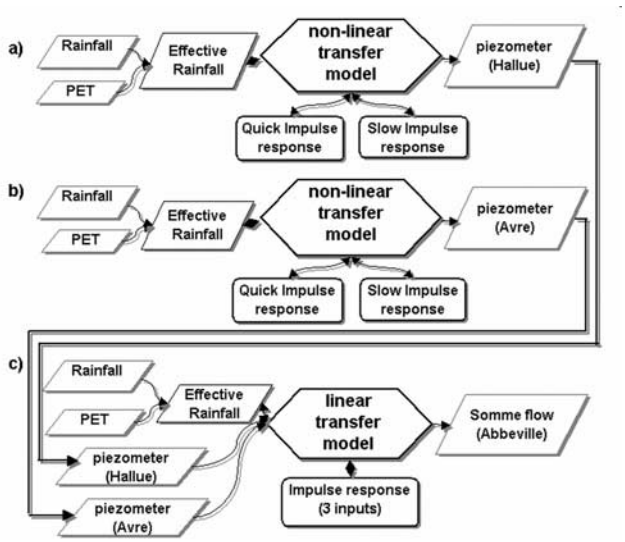

Figure 3. The architecture of the models used for (a) the pressure head in the fissured chalk from effective rainfall (p463X), (b) the pressure head in the riverbank sediments from effective rainfall (p624X), and (c) the Somme flow at Abbeville from effective rainfall and the pressure head in both the fissured chalk and the riverbank sediments. The three models used in cascade allow the calculation of the Somme flow from rainfall and potential evapotranspiration, taking into account the recharge and discharge of the chalk groundwater, as well as runoff.

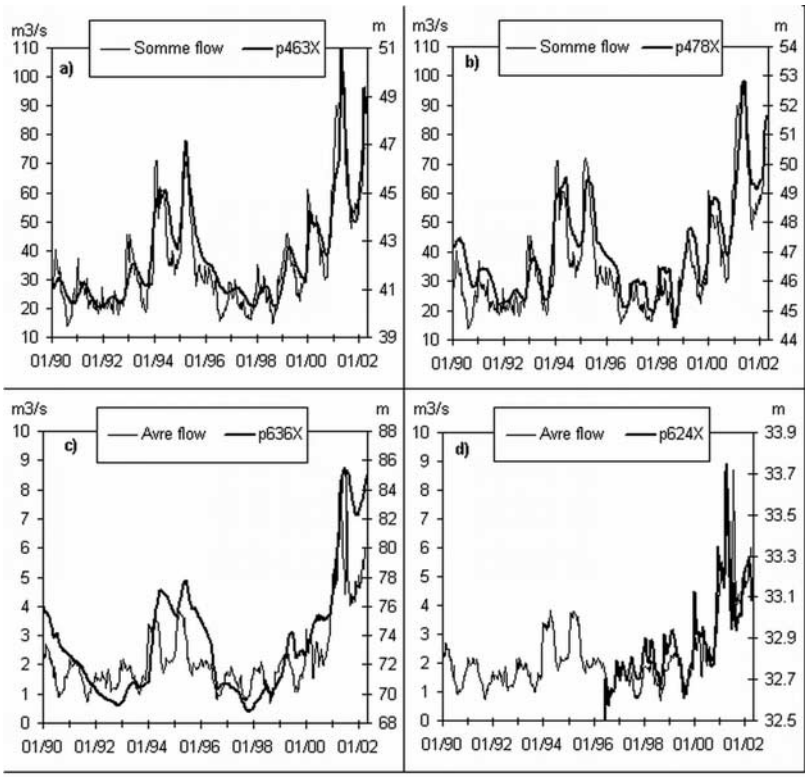

Figure 4. Comparison between piezometric levels, the Somme flow at Abbeville and the Avre flow at Moreuil. The vertical scale has been adapted to make comparison easier. Piezometers (a) p463X (Hallue catchment), (b) p478X (High Somme valley), and (c) p636X (Avre catchment) located on the slopes of the wet valleys. Their response anticipated the flooding of April 2001. (d) Piezometer p624X (Avre catchment), which is close to the Avre River and, consequently, is strongly influenced by the river water level. Pressure-head variations are very low compared to the other piezometers.

This behavior is characteristic of the water table beneath the plateaus where macropermeability is lower than in the fissured chalk aquifer with very efficient drainage.

5.2. Linear Processes

[14] Two piezometers are required as input for the third transfer model (Figure 3) to accurately reproduces the Somme flow after the flooding of April 2001. The recession curve reflects therefore the discharge of the different chalk aquifers whose pressure head remained very high for several months. Several couples of piezometers can be used. However, the model becomes increasingly stable, as the inputs are decorrelated. We use a couple comprising piezometer p463X (Hallue catchment) at the junction between the Somme and the Hallue valleys, and piezometer p624X (Avre catchment) close to the Avre River (Figure 1b). The former is located along the top of a wet valley, which confers a high response to nonlinear processes in the unsaturated zone, whereas the latter is strongly constrained by the surface water network and reflects interactions between riverbank sediments and the surface water network.

[15] Rainfall data measured at ten meteorological stations are used (Figure 1). A sum R_Σ of rainfall series is defined so as to optimize the contribution of every pluviometer into the transfer models. For every transfer model the output of which is the flow Q or the piezometric variations ΔH the cross correlogram $Cor_{R_\Sigma,Out}(\tau)$ of R_Σ and the output is maximized. From the weighted sum:

$$R_\Sigma = \sum_{k=1,p} \delta_k R_k \quad \delta_k \geq 0 \quad k = 1, \cdots, p \sum_{k=1,p} \quad \delta_k = 1 \qquad (1)$$

(p is the number of pluviometers) the cross correlogram $Cor_{R_\Sigma,Q}(\tau)$ of R_Σ and the output of the transfer model can be written as (the output is supposed to be Q):

$$Cor_{R_{\Sigma,Q}}(\tau) = \frac{\sum_{i=1,N} \left[R_\Sigma(t_i) - \overline{R_\Sigma}\right] \cdot \left[Q(t_i+\tau) - \overline{Q}\right]}{\sqrt{\sum_{i=1,N} \left[R_\Sigma(t_i) - \overline{R_\Sigma}\right]^2} \sqrt{\sum_{i=1,N} \left[Q(t_i) - \overline{Q}\right]^2}} \qquad (2)$$

where $\overline{R_\Sigma}$ and $\overline{Q}$ are the mean of R_Σ (t_i) and $Q(t_i)$, respectively (N is the number of sampling steps). The weighting factors δ_k are calculated so that they maximize the objective function (Figure 5):

$$O_\Sigma = \sum_{l=1,S} Cor_{R_{\Sigma,Q}}(\tau_l) \qquad (3)$$

defined from the increasing section of the cross correlogram $Cor_{R_\Sigma,Q}(\tau_1)$:

$$Cor_{R_{\Sigma,Q}}(\tau_n) \leq Cor_{R_{\Sigma,Q}}(\tau_m), 0 \leq \tau_n < \tau_m \leq \tau_S \qquad (4)$$

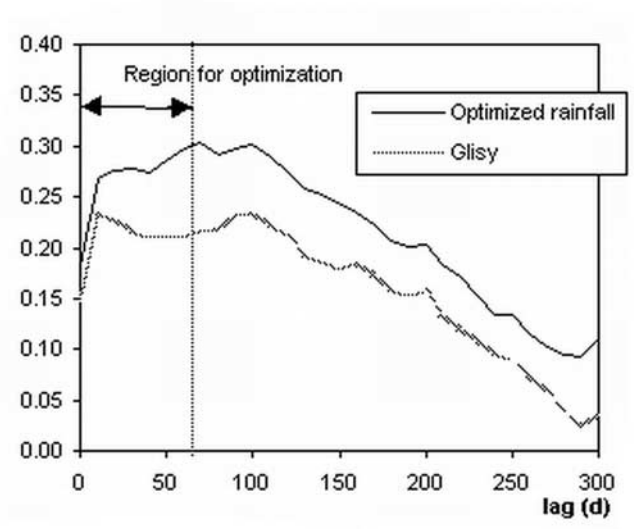

Figure 5. Representation of the rainfall-Somme flow cross correlogram for both the optimized rainfall $\mathbf{R}_\Sigma$ (equation (5)) and the rainfall observed at the Glisy station not included in the linear combination $\mathbf{R}_\Sigma$. The optimization is carried out from the increasing part of the cross correlogram, i.e., for $0 \leq \text{lag} \leq 60$ d.

The higher the objective function O_Σ, the stronger the causal relationship between the weighted rainfall series R_Σ and the output Q and, consequently, the more representative the combination of pluviometers.

[16] The linear combinations obtained for the Somme flow and the piezometers p463X and p624X from the ten meteorological stations are respectively:

$$R_\Sigma = 0.43 \times \text{Bernaville} + 0.35 \times \text{Meaulte} + 0.22 \times \text{Rouvroy} \quad (5)$$

$$R_\Sigma = 0.30 \times \text{Bernaville} + 0.25 \times \text{Meaulte} + 0.19 \times \text{Oisemont} + 0.26 \times \text{Rouvroy} \quad (6)$$

$$R_\Sigma = 0.40 \times \text{Bernaville} + 0.27 \times \text{Epehy} + 0.07 \times \text{Meaulte} + 0.26 \times \text{Rouvroy} \quad (7)$$

Those rainfall series are very similar since their Euclidian distance is less than 2.3 mm/10 d for every couple whereas it is 17 mm/10 d for the couple Bernaville, Rouvroy. Thus the short-term rainfall variations are extremely correlated at the catchment scale with a 10-day time step. Only a few numbers of pluviometers are required to represent rainfall on subcatchments as well as on the whole basin, which is confirmed when the linear combinations R_Σ are optimized from the flow of tributaries whatever the drained subcatchments. The more significant pluviometers are not necessarily located onto the corresponding subcatchments. Actually, the weights associated to the stations (5–7) show that short-term variations of rainfall are ruled by the winds of the northwest coming from the sea (Bernaville) while being influenced by the plateaus (Rouvroy, Epehy and Meaulte). Pluviometers are redundant since more than half of them have no significant contribution into the combinations R_Σ.

[17] The isohyets show significant variations of mean rainfall values over the catchment it rains more on the plateaus (22.1 mm/10 d at Epehy) than in the valleys (18.5 mm/10 d at Glisy). The mean rainfall values increase near the sea (23.0 mm/10 d at Abbeville, 25.6 mm/10 d at Vron). The variations reach 42% between extreme values. In order to integrate the heterogeneities of mean precipitation amounts onto the basin, the sums R_Σ are weighted adequately (the weighting factors are close to 0.7).

[18] Potential evapotranspiration is obtained from the Abbeville meteorological station. Contrarily to what occurs for rainfall series, the transfer models are not sensitive to the location where the potential evapotranspiration is measured since the relative variations of potential evapotranspiration are used. Considering the piezometric variations $\Delta\mathbf{H}_1$ and $\Delta\mathbf{H}_2$ expressed according to a reference level as representing the processes by which groundwater from both fissured chalk aquifers and riverbank sediments feed the Somme River, the following relationship can be written:

$$F(t) = S.\left[\lambda.\boldsymbol{\Gamma} * \mathbf{R}^s_{eff} + \lambda_1.\boldsymbol{\Gamma}_1 * \Delta\mathbf{H}_1 + \lambda_2.\boldsymbol{\Gamma}_2 * \Delta\mathbf{H}_2\right] + \varepsilon \quad (8)$$

where an asterisk represents the discrete convolution product, $F(t)$ is the flow of the Somme River at Abbeville, which is close to the outlet of the Somme basin, S is the catchment area, λ, λ_1, and λ_2 are weighting factors, and $\boldsymbol{\Gamma}$, $\boldsymbol{\Gamma}_1$, and $\boldsymbol{\Gamma}_2$ are normalized impulse responses (the area being unity), $\boldsymbol{\Gamma}$ is the transfer function of effective rainfall $\mathbf{R}^s_{eff}$ into the river as a consequence of runoff and $\boldsymbol{\Gamma}_1$ and $\boldsymbol{\Gamma}_2$ are transfer functions related to piezometers $\mathbf{H}_1$ and $\mathbf{H}_2$. Impulse responses $\boldsymbol{\Gamma}$, $\boldsymbol{\Gamma}_1$, $\boldsymbol{\Gamma}_2$ are defined on the interval $[0,\tau]$ so that

$$\begin{aligned}\Gamma(t_i) = {} & A.\exp\left(-\ln(2)((t_i - T)/D)^2\right) \\ & * \exp(-t_i.\ln(2)/L) \quad \text{if} \quad 0 \leq t_i \leq \tau \\ \Gamma(t_i) = {} & 0 \quad \text{if} \quad t_i > \tau \end{aligned} \quad (9)$$

This model is the expression of the recharge of a reservoir represented by the Gaussian $\exp(-\ln(2)((t_i - T)/D)^2)$ followed by its discharge represented by the exponential law $\exp(-t_i.\ln(2)/L)$. The succession of these two phenomena is then the convolution product of the recharge law by the discharge law. Parameter T represents the delay of the recharge process after a rainfall event, or a head impulse depending on the impulse response, whereas parameter D represents the duration of the recharge, L is the recession constant, A is the normalization constant. Because of its very small number of degrees of freedom (3 per impulse response), this parametric model produces better fits than a nonparametric solution when the observation period is short.

[19] For every piezometer, the reference level $\mathbf{H}^0$ from which are expressed the piezometric variations $\Delta\mathbf{H} = \mathbf{H} - \mathbf{H}^0$ corresponds to low storage. This reference level is estimated so that:

$$\mathbf{H}^0 = m - \beta.\sigma \quad (10)$$

where m and σ are the mean and the standard deviation of $\mathbf{H}$, respectively. The parameter β takes the value 2.5 when the regulation time of the piezometric level $\mathbf{H}$ is less than

1 year, which corresponds to a 160-year return period of $\mathbf{H}^0$ provided $\mathbf{H}$ follows a Gaussian distribution. The parameter β takes the value 3.95 when the regulation time is two years, the return period being 160^2 years if the climatic conditions of two successive years may be considered as independent. The actual value of β is interpolated according to the actual value of the regulation time, which is estimated from the $\mathbf{H}$ autocorrelogram.

[20] The random part ε represents erratic, complex, and usually short-term variability of the Somme River flow that is not explained by the model, including measurement errors, and whether they are due to instrumentation or sampling defects.

[21] Effective rainfall R^s_{eff} is calculated from rainfall R_Σ and the effective rainfall threshold Ω, such that [*Pinault et al.*, 2001a, 2001b]:

$$R^s_{eff}(t_i) = \begin{cases} R_\Sigma(t_i) - \Omega(t_i) & \text{if } R_\Sigma(t_i) \geq \Omega(t_i) \\ 0 & \text{if } R_\Sigma(t_i) < \Omega(t_i) \end{cases} \quad (11)$$

The effective rainfall threshold $\Omega(t_i)$ is related to both rainfall and potential evapotranspiration, such that

$$\mathbf{\Omega} = \mathbf{\Gamma}_{\Omega,PET} * \mathbf{PET} + \mathbf{\Gamma}_{\Omega,R} * \mathbf{R_\Sigma} + C^{st} \quad (12)$$

where $\mathbf{\Gamma}_{\Omega,PET}$ and $\mathbf{\Gamma}_{\Omega,R}$ are impulse responses of $\mathbf{\Omega}$ to potential evapotranspiration $\mathbf{PET}$ and to rainfall $\mathbf{R}_\Sigma$, respectively. These impulse responses are represented by trapezes with four degrees of freedom, with $\mathbf{\Gamma}_{\Omega,PET}$ being positive and $\mathbf{\Gamma}_{\Omega,R}$ being negative −rainfall induces a decrease in $\mathbf{\Omega}$, whereas potential evapotranspiration produces an increase in $\mathbf{\Omega}$. The inverse method aims to calculate the impulse responses $\mathbf{\Gamma}$, $\mathbf{\Gamma}_1$, $\mathbf{\Gamma}_2$, $\mathbf{\Gamma}_{\Omega,PET}$, $\mathbf{\Gamma}_{\Omega,R}$, the constant C^{st} and the factors λ, λ_1 and λ_2.

[22] Figure 6a displays a comparison between the observed Somme flow and the model (8). The discrepancies before and during the flood peak are due to both damaging of the equipment and the stream measurement when the river bursts its banks. The introduction of two piezometric levels $\Delta\mathbf{H}_1$ and $\Delta\mathbf{H}_2$ as inputs to the model allows the groundwater contribution to the Somme flow to be divided into two subcomponents. The contribution of groundwater from both the fissured chalk aquifer and the riverbank sediments slightly improves the fit between the model and the observed Somme flow. Since the piezometric levels $\Delta\mathbf{H}_1$ and $\Delta\mathbf{H}_2$ are considered to reflect the pressure head in the fissured chalk aquifer and the riverbank sediments, the components $S.\lambda_1.\mathbf{\Gamma}_1 * \Delta\mathbf{H}_1$ and $S.\lambda_2.\mathbf{\Gamma}_2 * \Delta\mathbf{H}_2$ represent the contributions of both these aquifers to the Somme flow, whereas the term $S.\lambda.\mathbf{\Gamma} * \mathbf{R}^s_{eff}$ concerns runoff. Nevertheless, this separation into two groundwater contribution components has no real interest because the riverbank sediments are fed by the chalk aquifer. The groundwater components are added together in Figure 6d, and the distinction between groundwater discharge and infiltration excess runoff shows that more than 80% of the Somme flow was supplied by groundwater during the flooding of 2001 and about 88% during the flooding of 2002, which is in good agreement with geochemical investigations [*Amraoui et al.*, 2002]. Figure 6e displays short impulse responses relative to both discharge groundwater and runoff. Nevertheless, the responses relative to groundwater discharge are more delayed than that relative to runoff because groundwater recharge occurs over several years (Figure 6d). The effective rainfall threshold $\mathbf{\Omega}$ is shown in Figure 6b. Impulse responses $\mathbf{\Gamma}_{\Omega,PET}$ and $\mathbf{\Gamma}_{\Omega,R}$ are represented in Figure 6f. Both impulse responses last for 50 days, which corresponds to the duration required by the soil moisture profile to regain equilibrium after a 10 day impulse (sampling rate), either a rainy period or an increase in evapotranspiration.

5.3. Nonlinear Processes

[23] Prediction of the Somme flow using the previous model requires rainfall-recharge models in order to characterize groundwater response in the chalk aquifer and the riverbank sediments, which is nonlinear (Figure 3). Such a model requires the solutions $\mathbf{\Gamma_s}$ and $\mathbf{\Gamma}_q$, the so-called slow and quick transfer functions, to the transport equation [*Pinault et al.*, 2001a]:

$$\Delta H(t_i) = 1/\eta\left[\mathbf{\Gamma}_s * \mathbf{R}_s + \mathbf{\Gamma}_q * \mathbf{R}_q\right] + \varepsilon \quad (13)$$

where η is a constant related to the effective porosity ω_s and ω_q of the aquifer: $\omega_s = \eta/\sup(\Gamma_s(t_i))$ and $\omega_q = \eta/\sup(\Gamma_q(t_i))$. Parameters ω_s and ω_q can thus be interpreted as the effective porosity as regards slow and quick transfer respectively. Impulse responses $\mathbf{\Gamma_s}$ and $\mathbf{\Gamma}_q$ are parametric models like (9).

[24] Effective rainfall $R^g_{eff}(t_i)$ is composed of two components $R^g_{eff}(t_i) = R_s(t_i) + R_q(t_i)$, $R_s(t_i)$ and $R_q(t_i)$, representing those parts of the rainfall that induce the slow and quick components of the recharge, respectively. Recharge $\Delta H(t_i)$ therefore is the combination of matrix-macropore flow. An increase in pressure head is observed for the piezometers located in the fissured chalk (Figures 1a and 1b) along the edge of the plateaus where the unsaturated zone is thick. The hydraulic gradient thus increases at the top of the slopes, with a pressure head capable of rising several meters over a short time, inducing a rapid groundwater discharge at the end of spring.

[25] Quick infiltration occurs only after exceptional rainfall, when hydraulic continuity is established between matrix and macropores. The component $R_q(t_i)$ may be expressed according to $R^g_{eff}(t_i)$ so that

$$R_q(t_i) = R^g_{eff}(t_i) \cdot \alpha(t_i) \quad (14)$$

where the function $\alpha(t_i)$ is the proportion of effective rainfall participating in quick transfer; $\alpha(t_i)$ that expresses the nonlinear switching behavior of groundwater recharge from matrix flow to macropore flow is related to the effective rainfall of previous events such that:

$$\alpha = \mathbf{\Gamma}_{\alpha,R_{eff}} * \mathbf{R}^g_{eff} \quad (15)$$

where $\mathbf{\Gamma}_{\alpha,R_{eff}}$ is the impulse response of $\alpha(t_i)$ to effective rainfall $\mathbf{R}^g_{eff}$ (Figure 7e). A trapeze with four degrees of freedom represents this impulse response. The function $\alpha(t_i)$ increases when several successive intense rainfall events occur as a result of the pile-up effect. This function expresses the filling up of fractures, which occurs when successive rainfall events are close enough to fill up the fractures, which competes with the drainage of macropores

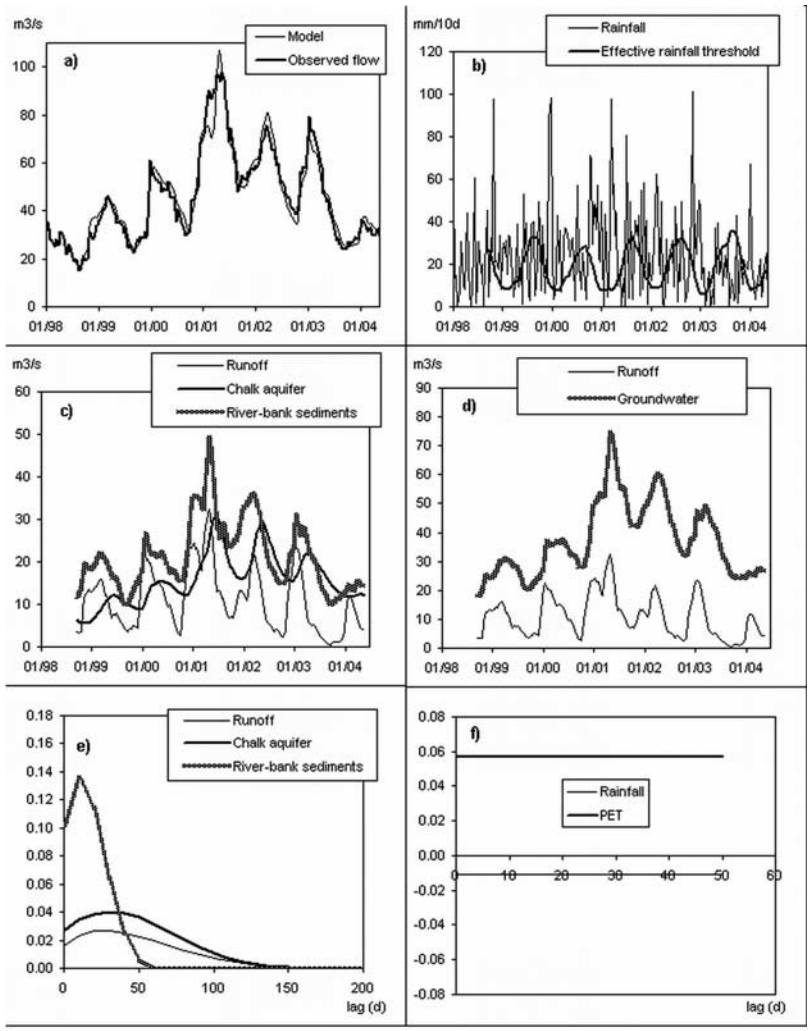

Figure 6. Inverse modeling of the Somme flow at Abbeville. Sampling rate is 10 days. (a) Comparison between modeled and observed flow. The Nash coefficient is 0.94 (b) The rainfall $\mathbf{R}_{\Sigma}$ and the effective rainfall threshold Ω. The rainfall-evaporation balance is $\overline{R}_{eff} = 0.45.\overline{R}$. (c) Hydrograph separation of the Somme flow into runoff and discharge from the chalk aquifer and the riverbank sediments. (d) Addition of the two groundwater-related components. (e) Impulse responses of the Somme flow to rainfall and piezometric levels. The former refers to runoff, whereas the latter represents discharge from the chalk aquifer and the riverbank sediments. The area of each component is proportional to its contribution to the Somme flow. (f) Impulse response of the runoff threshold Ω to rainfall and potential evapotranspiration (constant = −1.8 mm).

toward the surface water network. The impulse response $\mathbf{\Gamma}_{\alpha,R_{eff}}$ shows a plateau when the lag is between 0 and 50 days. The proportion of effective rainfall involved in quick transfer increases as soon as it rains and cancels when it does not rain for 50 days.

[26] By corollary, the component R_s (t_i) of the rainfall inducing the slow component of the transfer function may be written as:

$$R_s(t_i) = R^g_{eff}(t_i) \cdot (1 - \alpha(t_i)) \tag{16}$$

The inverse method aims to calculate the normalized impulse responses $\mathbf{\Gamma}_s$ and $\mathbf{\Gamma}_q$, as well as the impulse responses $\mathbf{\Gamma}_{\Omega,PET}$, $\mathbf{\Gamma}_{\Omega,R}$ and the constant C^{st} for calculating the effective rainfall threshold $\Omega(t_i)$ and the impulse response $\mathbf{\Gamma}_{\alpha,R_{eff}}$ for calculating the proportion of effective rainfall $\alpha(t_i)$ involved in quick flow [*Pinault et al.*, 2001a].

[27] The inverse model of groundwater recharge in fissured chalk is represented in Figure 7. The slow and quick impulse responses $\mathbf{\Gamma}_s$ and $\mathbf{\Gamma}_q$ clearly reflect the behavior of the fissured chalk in the unsaturated zone: long memory of the groundwater system is due to matrix flow, whereas quick transfer occurs when the macropores are water-saturated (Figure 7d). This is similar to the flush-flow effect that can be observed in karstic aquifers after heavy rainfall, when hydraulic continuity is established between the unsaturated and flooded zones. The pressure head rises suddenly, leading to groundwater discharge through macropores. The effective porosity calculated from (13) is $\omega_s = 4.5\%$ and $\omega_q = 1.1\%$.

[28] The mean transit time τ_i associated with the impulse response $\mathbf{\Gamma}_i$ is the mean value of the lag:

$$\tau_i = \sum_{n=0,\nu} \Gamma_i(n).n.\Delta t / \sum_{n=0,\nu} \Gamma_i(n) \tag{17}$$

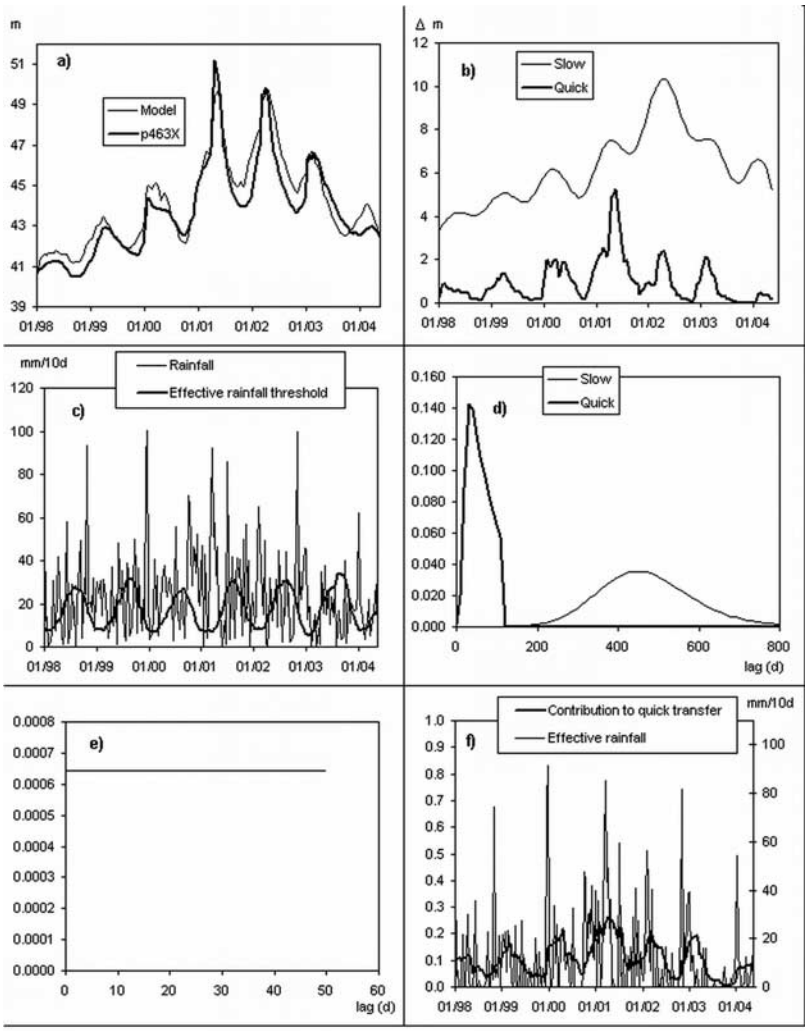

Figure 7. Inverse modeling of groundwater recharge in fissured chalk (piezometer p463X in the low Somme valley) with a sampling step of 10 days. (a) Comparison between the observed and modeled pressure heads. The Nash coefficient is 0.88. (b) The quick and slow components of the piezometric variations above the reference level (37 m). (c) The infiltration threshold Ω (t_i) used in calculating effective rainfall; 45.5% of total rainfall contributes to groundwater. (d) Slow and quick impulse responses $\mathbf{\Gamma}_s$ and $\mathbf{\Gamma}_q$. (e) The impulse response of $\alpha(t_i)$ to effective rainfall. (f) The contribution $\alpha(t_i)$ of effective rainfall to quick transfer.

where ν is the duration of the impulse response. τ_i is 57 days for quick transfer ceasing 120 days after the rainfall event, and 470 days for slow transfer lasting 800 days.

5.4. Flood Generation

[29] Quick transfer through the fractures occurs only for wet years and over a short time period (Figure 7b). The contribution of effective rainfall to quick transfer reached 30% during the rainy months of winter and spring 2001 (Figure 7f), taking part in flooding after the pressure head of the chalk groundwater increased drastically (Figure 7b). The peak was superimposed onto the slow component, which was very high in April and May 2001. Because of the successive wet years, pressure head had increased regularly since 1997 and certain piezometric levels soared in April 2001.

[30] On the other hand, discharge of the chalk groundwater is very rapid when pressure head is high due to macropermeability (Figure 6e). Hydrograph separation of the Somme flow is represented in Figure 6d. The mean runoff contribution to the Somme flow is 23%. The peak resulting from runoff triggered the flood process, with the maximum being reached at the beginning of April 2001. Groundwater discharge, whose maximum was reached at the end of May to the beginning of June 2001, then took over from runoff. The contribution of runoff, which was 30% on 5 April 2001, dropped to 20% at the end of June 2001. The flow did not fall below 80 m^3/s until the end of June because of discharge of the chalk groundwater.

[31] The flooding of 2002 occurred earlier in the year and was again generated by discharge of the chalk groundwater after being triggered by runoff. The flooding resulted from the high level of the chalk water table, as the low-water period during October and November 2001 was not sufficient to significantly decrease the level owing to the long memory of the groundwater system (Figure 7d). Nevertheless, consequences of the 2002 flood were very limited

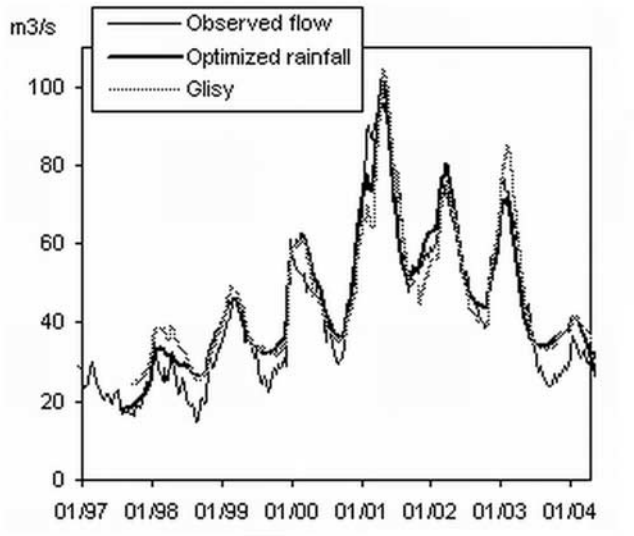

Figure 8. Comparison of the Somme flow model according to the rainfall series used as input: optimized rainfall $\mathbf{R}_\Sigma$ and rainfall at the Glisy station (the Nash coefficient is 0.92 and 0.88, respectively). Although the best fit is obtained from the optimized rainfall $\mathbf{R}_\Sigma$, rainfall series may be swapped to simulate the 2001 flood accurately because both models produce very similar estimations of the peak of the flow during the 2001 flood.

since exceptional rainfall occurred neither at the end of winter nor in spring, which hampered efficient switching from matrix flow to macropore flow.

5.5. Rainfall Generator

[32] Since the statistic analysis of streamflow requires a large number of series, a stochastic process is used consisting in the generation of rainfall and potential evapotranspiration, then piezometric levels via nonlinear transfer models and flows. Numerous rainfall generators have been developed for the last decade but they do not allow the control of nonstationarities. The precipitation generator that is presented here uses the Markov chain Monte Carlo and simulated annealing [*Bardossy*, 1998] from the Hastings–Metropolis algorithm [*Metropolis et al.*, 1953; *Hastings*, 1970]. This method is extended to the simulation of potential evapotranspiration series.

[33] The precipitation generator allows the random simulation of rainfall series, while respecting certain conditions deduced from the analysis of the observed rainfall series. To be able to simulate long-term fluctuations of rainfall, long observed rainfall series are required. The only rainfall series observed on the Somme basin that fulfills this requirement has been observed at the Glisy station. So, this rainfall series is used instead of the optimized series R_Σ to analyze the response of the Somme basin to nonstationarities of climatic inputs, as the flood is still reproduced accurately (Figure 8).

[34] The rainfall generator is defined from the following five properties: First is marginal distribution of the precipitation amount, corresponding to the sampling step Δt (10 days). The Gumbel law is used to sample exceptional events (Figure 9). The second is the density of events (mean number of events per unit time). The third is autocorrelation function of the precipitation amount. Fourth is the scaling relationship using the first three raw moments of the aggregated distribution fulfilled for k = 1, 2 and 3, Δt = 10, 20 and 30 days

$$M_j(k.\Delta t) = k^{\lambda(j)} M_j(\Delta t) \tag{18}$$

where the moment $M_j(k.\Delta t)$ is the sum, on the time period $k.\Delta t$, of the precipitation amount raised to the power of j. Only strictly positive sums are considered. This scaling relationship aims to structure the duration of wet periods. The fifth is probability density of the monthly precipitation amount. Two other constrains are added to those classical properties: (1) temporal variability of precipitation averaged over characteristic time steps whose duration is chosen to emphasize nonstationarities of climatic inputs and (2) meteorological forecast.

[35] The rainfall series is generated in the following way. A period of time τ is defined as follows.

[36] 1. Each event is allocated a precipitation amount drawn randomly from the marginal distribution.

[37] 2. The events are evenly distributed over the period τ until the mean annual precipitation amount matches with the observations.

[38] 3. The events are temporally organized by performing successive swaps of precipitation events (including absence of rainfall). The aim is to minimize an objective function chosen so that the criteria defining the temporal structure of the simulated series converge to those of the observed series. Each swap that decreases the objective function is confirmed. In the opposite case, the swap is confirmed only with probability

$$\exp((O_0 - O)/T) \tag{19}$$

where the difference between the objective functions before and after permutation $O_0 - O$ reflects the 'degradation' of the temporal properties of the simulated series (actual objective functions are defined in equations (20)–(25)). Temperature T is a number that decreases regularly as soon as the thermodynamic equilibrium (or "freezing") is reached after M attempted swaps, i.e., when the swaps no longer significantly alter the objective function. The lower the annealing temperature T (by analogy with metallurgy), the lower the probability of a nonimproving swap. This generator becomes increasingly effective when the series to be simulated contains a large number of events, enabling a large number of swaps.

[39] The objective function for the autocorrelation function is the squared difference between a prescribed $\rho^*(t)$ and the simulated $\rho(t)$:

$$O_1 = \sum_{k=1,K} (\rho^*(k\Delta t) - \rho(k\Delta t))^2 \tag{20}$$

where K is the number of lags.

[40] For the scaling relationship the objective function is the squared difference between a prescribed exponent $\lambda^*(j)$ and the simulated $\lambda(j)$ for j = 1, 2, 3:

$$O_2 = \sum_{j=1,3} \left(\lambda^*(j) - \lambda(j)\right)^2 \tag{21}$$

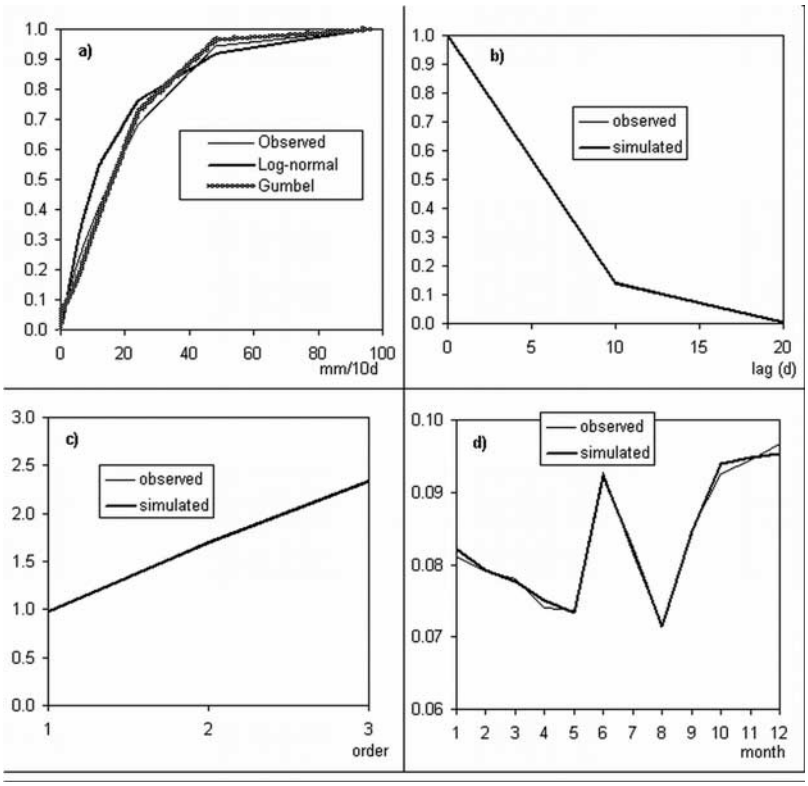

Figure 9. Properties of precipitation amount and potential evapotranspiration established over the period 1929–2003 (Glisy station). (a) Marginal probability (distribution function) of the precipitation amount. The Gumbel law is used for the probability $P \geq 0.95$. (b) Autocorrelation functions of precipitation amount. (c) Exponent of scaling relationship versus order of the moment (precipitation amount). (d) Probability density of monthly precipitation amount.

For the seasonality of precipitation the objective function is

$$O_3 = \sum_{k=1,12} \left(\overline{R}_k^* - \overline{R}_k\right)^2 \tag{22}$$

where $\overline{R}_k^*$ and $\overline{R}_k$ are the prescribed and simulated mean rainfall amounts corresponding to the month k.

[41] For the nonstationarities of precipitation the objective function is:

$$O_4 = \sum_{k=1,K} \left(\overline{R}_k^* - \overline{R}_k\right)^2 \tag{23}$$

where $\overline{R}_k^*$ and $\overline{R}_k$ are the prescribed and simulated mean rainfall amounts calculated according to the characteristic time step k, i.e., the timescale of precipitation fluctuations to be simulated. K is the number of characteristic time steps. For the meteorological forecast the objective function is the random number:

$$O_5 = \left(R_k^* - R_k\right)^2, k \in 1, \cdots, N \tag{24}$$

For every simulated series, the index k is drawn randomly so that the probability that $k = i (i = 1, \cdots, N)$ is the confidence level $\mu_i (\sum_{i=1,N} \mu_i = 1)$ of the forecast $R_k^* = R_i$; R_i is the precipitation amount forecasted with a confidence level μ_i. Finally, these objective functions are combined:

$$O = \beta_1 O_1 + \beta_2 O_2 + \beta_3 O_3 + \beta_4 O_4 + \beta_5 O_5 \tag{25}$$

the positive weights $\beta_1 \cdots, \beta_5$ being used to normalize the objective function. Figure 9 shows the characteristic properties of the precipitation amount; rainfall is simulated over a 20-year period.

5.6. Potential Evapotranspiration Generator

[42] In order to reproduce accurately the nonstationarities of climatic inputs due to possible climate changes, a potential evapotranspiration generator coupled to the rainfall generator is presented. Although simulated annealing is still used for potential evapotranspiration, it is the deviations of potential evapotranspiration around the mean monthly values (noise) that are simulated. Since these deviations are temporally structured, simulated annealing enables the observed and simulated autocorrelation functions to be as close as possible, as well as the cross-correlation noise–precipitation amount functions and the standard deviation of noise estimated for each month. The cross-correlation noise–precipitation amount function is calculated for positive and negative lags in order to simulate both the causal relationship of temperature on rainfall and the inverse. Here again, the meteorological forecast can be taken into account to force the mean potential evapotranspiration over a predefined period. The standard deviation of noise generally undergoes monthly variations. It is close to zero in winter because of very low potential evapotranspiration, whereas the variation amplitude can be high in summer. The first three moments are calculated from the absolute value of

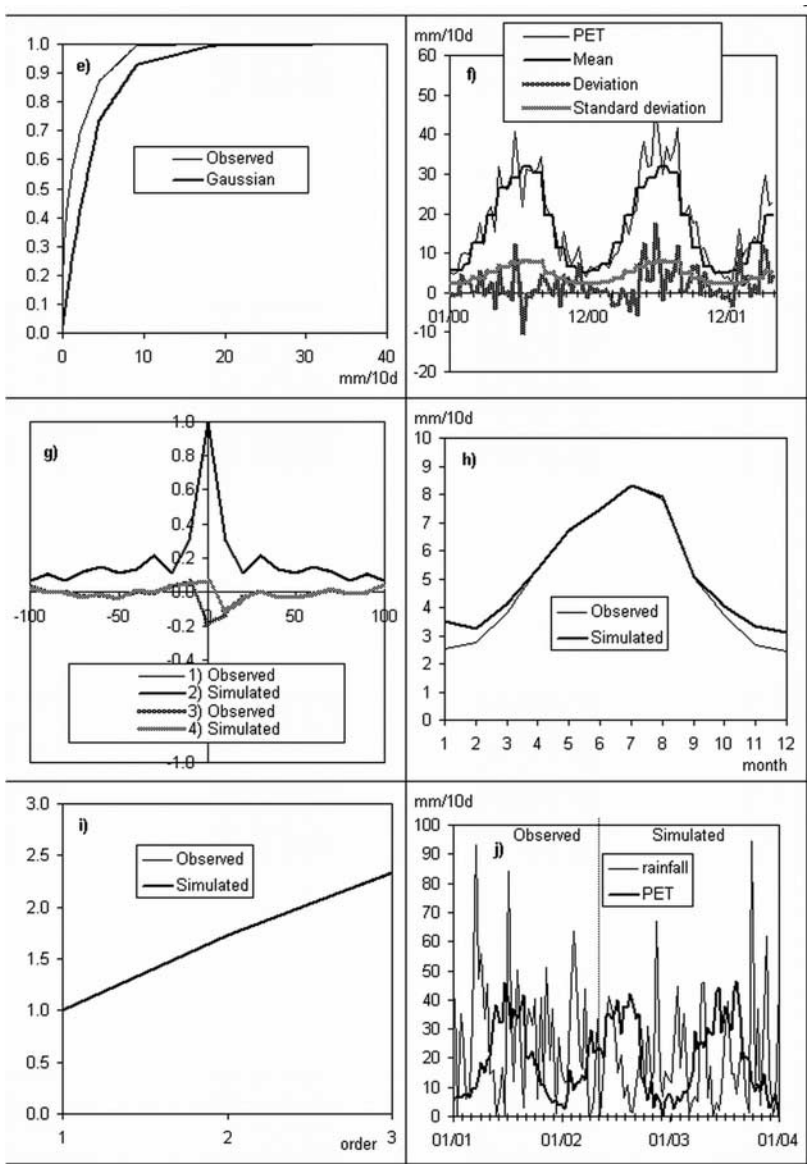

Figure 10. (a) Marginal probability (distribution function) of potential evapotranspiration (Abbeville station). The Gaussian law is used for the probability $P \geq 0.95$. (b) Representation of the deviation (noise) of potential evapotranspiration according to the monthly average calculated over the whole observation period. Standard deviation of noise is also represented, showing a strong seasonality. (c) Autocorrelation (1, 2) of the noise of potential evapotranspiration and cross correlation (3, 4) of noise and rainfall. (d) Standard deviation of noise of potential evapotranspiration. (e) Exponent of scaling relationship versus order of the moment (noise of potential evapotranspiration). (f) Rainfall and potential evapotranspiration.

deviations. Calculation of moments from the signed deviations would therefore lead to zero values when the observation period increases because the mean value of deviations tends to zero, making the exponents $\lambda(j)$ meaningless.

[43] Adding the simulated noise to the monthly average of potential evapotranspiration generates potential evapotranspiration series. The noise is simulated as follows.

[44] 1. A potential evapotranspiration deviation, drawn randomly from the observed marginal distribution, is allocated to each sampling step $k.\Delta t$. Exceptional events are sampled from a Gaussian law (Figure 10). A sign is allocated using the binary random variable evenly distributed on [0,1].

[45] 2. As for rainfall generation, simulated annealing is used to temporally organize the deviations. The objective functions O_1, O_2, O_5 are similar to the previous ones. The objective function O_3 is applied here to the monthly standard deviation of noise. A new objective function O'_1 refers to the cross correlation ρ' between precipitation amounts and potential evapotranspiration deviations:

$$O'_1 = \sum_{k=1,K} \left(\rho^{*\prime}(k\Delta t) - \rho'(k\Delta t) \right)^2 \qquad (26)$$

After simulated annealing is performed on the precipitation amounts, swapping potential evapotranspiration deviations

(rainfall amounts remain fixed) minimizes this objective function. Figure 10 shows the characteristic properties of the potential evapotranspiration deviations.

5.7. River Flow Generator

[46] Generation of the Somme flow is performed by using the cluster models (Figure 3). Each realization is obtained by simulating both precipitation amounts and potential evapotranspiration as model inputs. Piezometric levels in the chalk aquifer and the riverbank sediments are calculated, then the Somme flow from the third model where the previous results are used as inputs.

6. General Analysis of Results and Discussion

[47] In order to emphasize the response of the Somme Basin to nonstationarities of climatic inputs, four rainfall generators are used whose parameters are based on the analysis of two periods, 1929 to 2002 for the first two generators designed to simulate stationary climate and 1984 to 2002 for the last two generators designed to simulate climate changes. Before 1929, the rainfall records are monthly and thus cannot be used in the inverse model that has a sampling interval of 10 days.

[48] The short-term variance, i.e., the variance in precipitation cumulated over 2-month intervals so as to avoid any significant difference over the two observation periods, is predefined in the first rainfall generator. Under such conditions, the standard deviation and the mean are respectively 44 mm and 107 mm for the 1929–1983 period, and 46 mm and 109 mm for the 1984–2002 period; both values are not significantly different for the two periods. The maximum rainfall height over 10 days considered in the marginal distribution is 100 mm, that observed from 10 to 19 November 1972. The short-term variance is again predefined in the second rainfall generator, but the maximum rainfall height over 10 days is 120 mm, that observed from 1 to 10 November 2002.

[49] In the third rainfall generator it is the long-term variance, i.e., the variance in precipitation cumulated over 2-year intervals during the 1984–2002 period, that is predefined. Standard deviation and the mean are respectively 170 mm and 1280 mm for the 1929–1983 period, and 227 mm and 1330 mm for the 1984–2002 period, thus revealing a considerable increase in long-term variability but very similar means. The long-term variability increase is due to the drought conditions prevailing over the three consecutive years in 1989, 1990 and 1991 followed by successive wet years in 1999, 2000, 2001 and 2002. The maximum 10-day rainfall height is 100 mm, as in the first generator. The long-term variance is again predefined in the fourth rainfall generator, but the maximum 10-day rainfall height is 120 mm, as in the second generator.

[50] The stochastic process consists in generating a large number of rainfall and potential evapotranspiration series, from which are deduced piezometric levels representative of groundwater in the chalk aquifer and in the riverbank sediments, then the Somme flow via the transfer models. The rainfall generators are constrained by the global conditions (18)–(22) as well as by the particular condition (23) that confers the characteristic of each generator. This stochastic process is analyzed from 4000 realizations to estimate both the conditional and the unconditional probabilities of occurrence of flooding P, from which are estimated the return periods $T = 1/P$. To determine the unconditional probability, four hydrological cycles are considered between the date of forecast and flooding in order to make the hydrosystem independent of the initial state. The first and the fourth generators are used to estimate the conditional probability of occurrence of flooding, i.e., the probability of overreaching a critical flow at a given time when the prevision is carried out before flooding. The conditional probability of occurrence of flooding is a crucial issue to manage population and goods. Two floods are analyzed, those that occurred in April–May 2001 and March–April 2002.

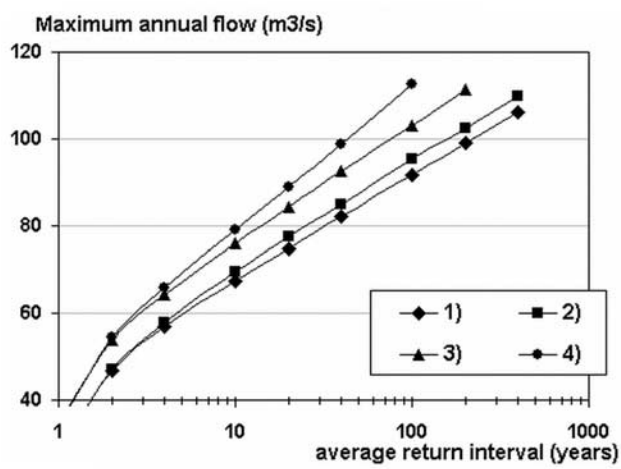

Figure 11. The average return interval of annual maximum flow estimated for each generator: (1) predefined short-term variance, maximum rainfall height over a 10-day period is 100 mm; (2) predefined short-term variance, maximum 10-day rainfall is 120 mm; (3) predefined long-term variance, maximum 10-day rainfall is 100 mm; and (4) predefined long-term variance, maximum 10-day rainfall is 120 mm.

6.1. Unconditional Probability of Occurrence of Flooding

[51] A 100- or 70-year return interval is obtained for a flow greater than 90 m^3/s with generators 1 and 2, which is compatible with the absence of flooding during the 20th century (Figure 11). For this same flow, the return interval decreases to 40 or 20 years with generators 3 and 4. A 300- or 200-year return interval is obtained for a flow greater than 104 m^3/s with a predetermined short-term variance (generators 1 and 2). Nevertheless, the simulated peak occurs earlier and for a shorter duration than the 2001 flood. The return interval of a late and durable flood is greater because multiyear rainfall fluctuations are extremely rare when the short-term variance is predefined, which is compatible with the absence of groundwater-induced flooding for more than five centuries. With a predetermined long-term variance (generators 3 and 4), the return interval decreases to 100 or 50 years depending on the maximum 10-day rainfall height used in the distribution, thus rendering an almost impossible event likely at human life scale.

[52] Thus macropore dominated hydrological systems appear to be very sensitive to nonstationarities of climatic

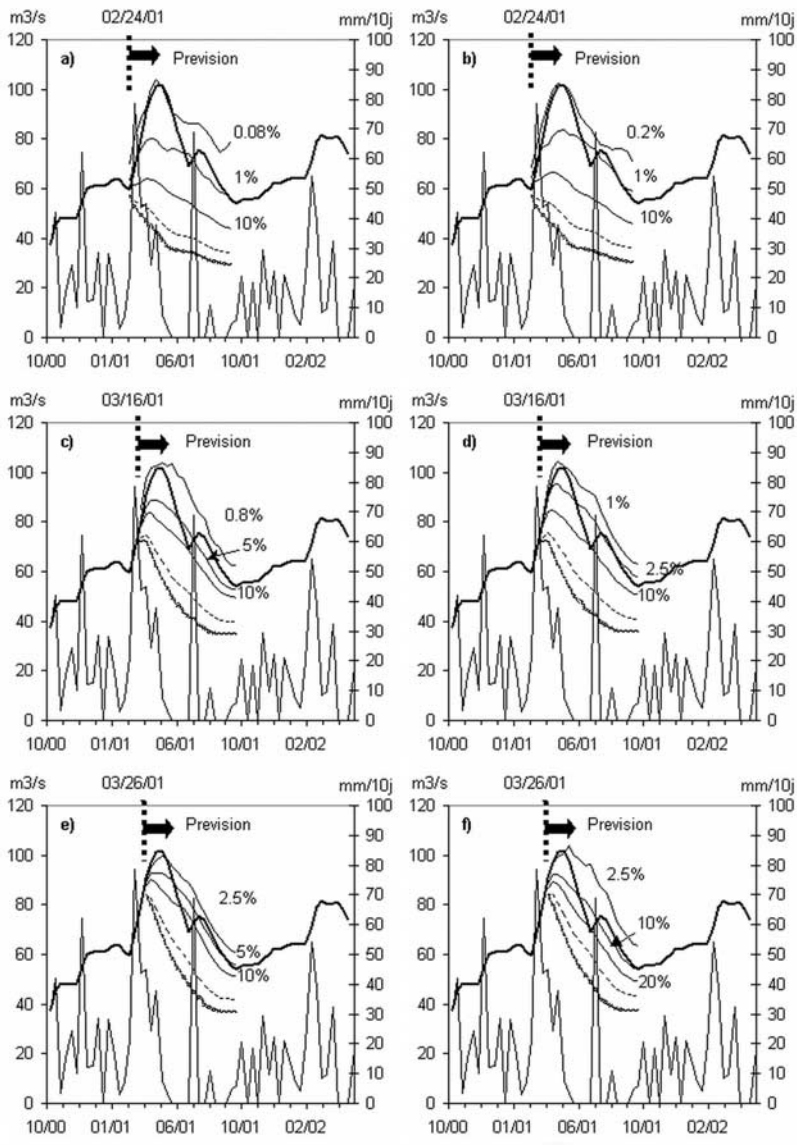

Figure 12. Representation of percentiles: prediction of the 2001 flooding performed for different times. The median is represented by a dashed line, and the 90th percentile is represented by a gray line. Other percentiles are shown explicitly. The mean precipitation amount for the basin is 19.4 mm per decade. (a, c, and e) Stationary climatic model. (b, d, and f) Climate change model.

inputs. Such systems accumulate groundwater in the unsaturated and in the saturated zones when multiyear rainfall fluctuations occur and may restore water suddenly when exceptional short-term rainfall events in winter and in spring threshold the drainage of matrix-micropores through the interconnected fracture network. Such exceptional short-term events generally occur locally, which may explain why the 2001 flood was limited to the Somme basin whereas a large part of the Paris Basin, Belgium and the South of England are vulnerable. Moreover, the Somme basin has a very low drainage capability since the slope of the Somme valley is low (Figure 1).

6.2. Conditional Probability of Occurrence of Flooding

[53] The probability of exceeding a flow of 104 m^3/s, forecasted on 27 October 2000 at a time when the pressure head of the chalk groundwater was already high owing to the precipitation amount in 1999, is 0.7% or 2.5% depending on the climate hypothesis. Figure 12 shows how the first flood can be forecasted with both models just before and during the exceptional precipitation that occurred between 6 March 2001 and 15 May 2001 (348 mm whereas the expected value for this period is 136 mm). The nonlinear behavior of the Somme flow amplifies the spacing of the percentiles for low probabilities. The probability of occurrence of a flow of 104 m^3/s on 24 February, i.e., just before the heavy rainfall, is 0.08% or 0.2% depending on the model (Figures 12a and 12b). Probability increases on 16 March, respectively 0.8% and 1% for a flow of 104 m^3/s or 5% in both models for a flow of 90 m^3/s (Figures 12c and 12d). Nevertheless, prediction undervalues the risk of flooding over the rainy period the probability it lasts so long with such a precipitation amount being very small. Low probabilities increase on 26 March, i.e., 10 days before flooding, 2.5%

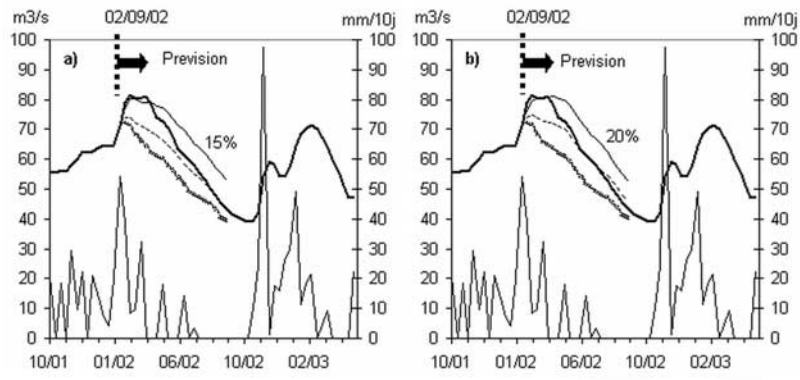

Figure 13. As in Figure 12, but prediction of the 2002 flooding performed for different times. (a) Stationary climatic model. (b) Climate change model.

for a flow of 104 m^3/s, or about 10% for a flow of 90 m^3/s in both models (Figures 12e and 12f). At this time, the rainy period is not yet over. So, the probability of occurrence of flooding resulting from a flow higher than 90 m^3/s increases 20 days before the peak and the difference between the two models becomes indistinct.

[54] The peak of 2002 was caused by the concomitance of a high precipitation amount in winter and groundwater discharge, the piezometric level of groundwater still being very high under the plateaus during winter 2002. Assuming a stationary climate, the probability of the flow exceeding 80 m^3/s in 2002, a flow that was effectively reached in early March is estimated at 15% or 20% (depending on the model) for 9 February 2002, i.e., during the rainy period and 3 weeks before the peak (Figures 13a and 13b). This 2002 flood, which induced very limited damage is much easier to predict than the previous 2001 flood because the mechanisms involved in flood generation are linear.

7. Conclusion

[55] Although the evolution of climate observed since the 1980s may be transient, evidence to suggest that the 2001 groundwater-induced flooding reflects climate changes is nevertheless strong, due to the extreme rarity of this catastrophic event. The average return interval of catastrophic flooding tightly depends on the amplitude of long-term rainfall fluctuations. The basin responds as a filter that is sensitive to rainfall fluctuations over a multiyear timescale. The response is all the more amplified, as exceptional events at a 10-day timescale are more frequent. Accumulated wetness over several years cause a rise in the chalk water table as a result of slow transfer in the unsaturated zone. The conductive fracture network becomes saturated after abundant rainfall, draining matrix micropores and forming continuity between the unsaturated zone and the groundwater, and thus speeding up the groundwater discharge into the surface water network. This flush-flow effect results from a rapid increase in groundwater pressure head.

[56] No recent anthropic modifications in the catchment that could have enhanced the flood may be referred to since the transfer model fits the Somme flow accurately since 1963. The only discrepancy is observed in 2001 just before the flood. Eventual transfers between the Seine and the Somme basins via the navigation canals cannot explain this flow excess as we checked from transfer models developed jointly for the Somme and the Oise basins. This discrepancy may be due to gauging station defects. On the other hand, the under estimate of the flow during the flood is due to the expansion of water out of the river banks, making the gauging curve biased. This assertion holds true for long-term evolutions of the Somme Basin that occurred over previous centuries due to the duration of flooding during which groundwater discharge is taken over from runoff. Moreover, the recession curve observed after the 2001 peak is clearly explained by the model; the canalized Somme River fulfilled its drainage function correctly, while the surface water network was supplied with groundwater discharge.

[57] The streamflow forecast would have helped the management of the crisis before the 2001 flood. Indeed, the percentiles tighten 20 days before the peak flow while the prevision no longer depends on the climatic model. At this stage, taking into account meteorological forecast would have greatly improved the reliability of the prevision after the peak of precipitation that occurred in March. The prevision is therefore extremely influenced by the tail of the rainy period as a result of the strong nonlinearities in the catchment response. The results of this study have implications for flood risk assessment and stress the need to evaluate long-term risks as a result of groundwater-induced flooding. Other basins that may not appear particularly prone to flooding could also be subjected to similar groundwater-induced flooding should the nonstationarities of climatic inputs observed in the north of France persist. Particularly vulnerable is the north of France, Belgium and England where macropore dominated hydrological systems are widespread.

[58] **Acknowledgment.** This work was supported by the BRGM's research grant within the flood project and the Direction Régionale de l'Environment de Picardie, France.

References

Amraoui, N., C. Golaz, V. Mardhel, P. Negrel, V. Petit, J.-L. Pinault, and T. Pointet (2002), Simulation par modèle des hautes eaux de la Somme, *Rep. BRGM/RP-51827-FR*, 184 pp., Bur. de Rech. Géol. et Minières, Orléans, France.

Amraoui, N., C. Golaz, V. Mardhel, and J.-L. Pinault (2003), Evaluation du risque d'inondation dans le bassin de la Somme: Apport de l'approche globale et de l'approche distribuée, paper presented at SIRNAT—Jour-

nées prévention risques naturels, 3ème, Bur. de Rech. Géol. et Minières, Orléans, France.

Bardossy, A. (1998), Generating precipitation time series using simulated annealing, *Water Resour. Res.*, *34*(7), 1737–1744.

Blazkova, S., and K. Beven (2002), Flood frequency estimation by continuous simulation for a catchment treated as ungauged (with uncertainty), *Water Resour. Res.*, *38*(8), 1139, doi:10.1029/2001WR000500.

Boyle, D. P., H. V. Gupta, S. Sorooshian, V. Koren, Z. Zhang, and M. Smith (2001), Toward improved streamflow forecasts: Value of semidistributed modeling, *Water Resour. Res.*, *37*(11), 2749–2760.

Buishand, T. A., and T. Brandsma (2001), Multisite simulation of daily precipitation and temperature in the Rhine basin by nearest-neighbor resampling, *Water Resour. Res.*, *37*(11), 2761–2776.

Champion, M. (2001), *Les inondations en France du VIe siècle à nos jours* [CD-ROM], Cent. Natl. du Machinisme Agricole du Génie Rural, des Eaux et des Forêts, Antony, France.

Chandler, R. E., and H. S. Wheater (2002), Analysis of rainfall variability using generalized linear models: A case study from the west of Ireland, *Water Resour. Res.*, *38*(10), 1192, doi:10.1029/2001WR000906.

Cowpertwait, P. S. P., C. G. Kilsby, and P. E. O'Connell (2002), A space-time Neyman-Scott model of rainfall: Empirical analysis of extremes, *Water Resour. Res.*, *38*(8), 1131, doi:10.1029/2001WR000709.

Crampon, N., J. C. Roux, and P. Bracq (1993), Hydrogeology of the chalk in France, in *The Hydrogeology of the Chalk of North-West Europe*, edited by R. A. Downing, M. Price, and G. P. Jones, pp. 81–123, Oxford Univ. Press, New York.

Deneux, M., and P. Martin (2001), Rapport de la commission d'enquête sur les crues de la Somme, *Sénat*, *34*, 606 pp.

Franks, S. W., and G. Kuczera (2002), Flood frequency analysis: Evidence and implications of secular climate variability, New South Wales, *Water Resour. Res.*, *38*(5), 1062, doi:10.1029/2001WR000232.

Gardner, C. M. K., J. D. Cooper, S. R. Wellings, J. P. Bell, M. G. Hodnett, S. A. Boyle, and M. J. Howard (1990), Hydrology of the unsaturated zone of the chalk of south-east England, in *Proceedings of the International Chalk Symposium*, pp. 611–618, Thomas Telford, London.

Georgakakos, A. P., H. Yao, M. G. Mullusky, and K. P. Georgakakos (1998), Impacts of climate variability on the operational forecast and management of the upper Des Moines River basin, *Water Resour. Res.*, *34*(4), 799–822.

Goel, N. K., R. S. Kurothe, B. S. Mathur, and R. M. Vogel (2000), A derived flood frequency distribution for correlated rainfall intensity and duration, *J. Hydrol.*, *228*, 56–67.

Haria, A. H., M. G. Hodnett, and A. C. Johnson (2003), Mechanisms of groundwater recharge and pesticide penetration to a chalk aquifer in southern England, *J. Hydrol.*, *275*, 122–137.

Hastings, W. K. (1970), Monte Carlo sampling methods using Markov chains and their applications, *Biometrika*, *57*, 97–109.

Hubert, P. (2001), La crue et les inondations de la vallée de la Somme de mars à mai 2001, report, Cons. Gén. de la Somme, Amiens, France.

Jain, S., and U. Lall (2001), Floods in a changing climate: Does the past represent the future?, *Water Resour. Res.*, *37*(12), 3193–3206.

Latraverse, M., P. F. Rasmussen, and B. Bobée (2002), Regional estimation of flood quantiles: Parametric versus nonparametric regression models, *Water Resour. Res.*, *38*(7), 1095, doi:10.1029/2001WR000677.

Lefrou, C. (2001), Les crues d'avril 2001 du bassin de la Somme, report, Conseil Général de la Somme, Amiens, France.

Mahmood-ul-Hassan, M., and P. J. Gregory (2002), Dynamics of water movement on Chalkland, *J. Hydrol.*, *257*, 27–41.

Metropolis, N., A. Rosenbluth, M. Rosenbluth, A. Teller, and E. Teller (1953), Equation of state calculation by quick computing machines, *J. Chem. Phys.*, *21*, 1087–1092.

Morrison, J. E., and J. A. Smith (2002), Stochastic modeling of flood peaks using the generalized extreme value distribution, *Water Resour. Res.*, *38*(12), 1305, doi:10.1029/2001WR000502.

Peters, R. R., and E. A. Klavetter (1988), A continuum model for water movement in a unsaturated fractured rock mass, *Water Resour. Res.*, *24*, 416–430.

Pinault, J.-L. (2001), Manuel utilisateur de TEMPO: Logiciel de traitement et de modélisation des séries temporelles en hydrogéologie et en hydrogéochimie. Projet Modhydro, *Rep. BRGM/RP-51459–FR*, 221 pp., Bur. de Rech. Géol. et Minières, Orléans, France.

Pinault, J.-L., H. Pauwels, and C. Cann (2001a), Inverse modeling of the hydrological and the hydrochemical behavior of hydrosystems: Application to nitrate transport and denitrification, *Water Resour. Res.*, *37*(8), 2179–2190.

Pinault, J.-L., V. Plagnes, L. Aquilina, and M. Bakalowicz (2001b), Inverse modeling of the hydrological and the hydrochemical behavior of hydrosystems: Characterization of karst system functioning, *Water Resour. Res.*, *37*(8), 2191–2204.

Price, M., R. A. Downing, and W. M. Edmunds (1993), The chalk as an aquifer, in *The Hydrogeology of the Chalk of North-West Europe*, pp. 35–58, Oxford Univ. Press, New York.

Price, M., R. G. Low, and C. McCann (2000), Mechanisms of water storage and flow in the unsaturated zone of the chalk aquifer, *J. Hydrol.*, *223*, 54–71.

Roux, J.-C. (1978), *Notice de l'atlas hydrogéologique de la Somme*, BRGM Ed., Orléans, France.

Thiery, D., N. Amraoui, and C. Golaz (2004), Etude des risques de crues dans le bassin de la Somme. Analyse par modélisation hydrodynamique spatialisée et prévisions par modélisation hydrologique globale, paper presented at Atelier sur la modélisation et la prévision des crues, Serv. Cent. Hydro-météorol. d'Appui à la Prévision des Inondations, Toulouse, France.

Veneziano, D., and V. Iacobellis (2002), Multiscaling pulse representation of temporal rainfall, *Water Resour. Res.*, *38*(8), 1306, doi:10.1029/2001WR000372.

Wellings, S. R. (1984), Recharge of the upper chalk aquifer at a site in Hampshire, England, 1. Water balance and unsaturated flow, *J. Hydrol.*, *69*, 259–273.

N. Amraoui, C. Golaz, and J.-L. Pinault, Water Research Division, Bureau de Recherches Géologiques et Minières, 3 avenue Claude Guillemin, F-45060 Orléans Cedex 2, France. (jlpinault@brgm.fr)

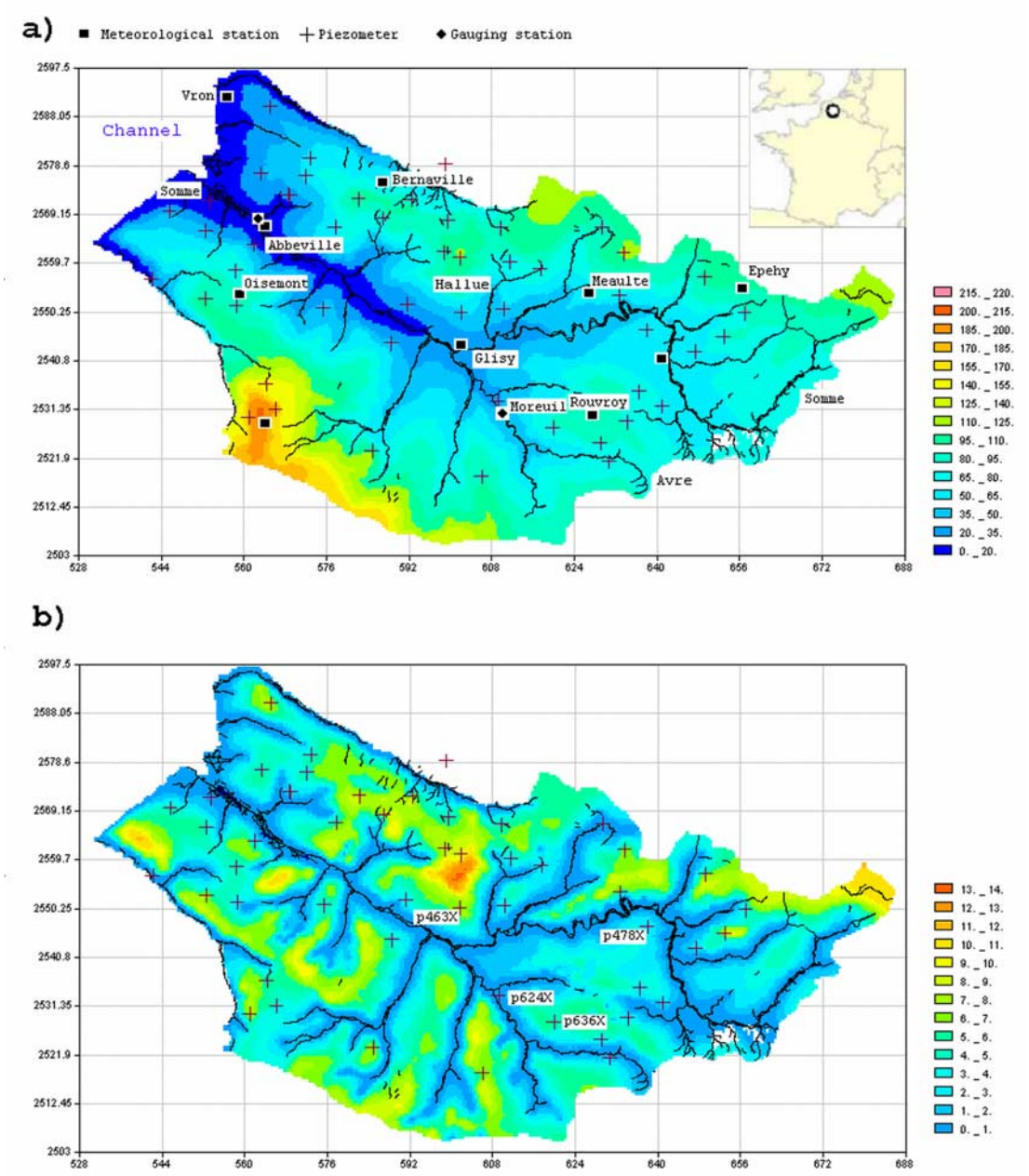

Figure 1. (a) Piezometric map and some equipment of the Somme Basin. Piezometric levels are calculated from 57 piezometers (hydrodynamic modeling with MARTHE software [*Amraoui et al.*, 2003; *Thiery et al.*, 2004]). Among the meteorological stations the Glisy station has produced data since 1900 with an interruption during the first World War. (b) Piezometric map and some equipment of the Somme Basin. Difference in piezometric levels between April 2001 (high storage) and December 2000 (low storage) is shown. The piezometers whose increase anticipated the flooding of April 2001 are located on the slopes of the wet valleys.